Lattice dynamics of the heavy-fermion compound URu_2Si_2

J. Buhot, M. A. Méasson,* Y. Gallais, M. Cazayous, and A. Sacuto
Laboratoire Matériaux et Phénomènes Quantiques, UMR 7162 CNRS, Université Paris Diderot, Bât. Condorcet 75205 Paris Cedex 13, France

F. Bourdarot, S. Raymond, G. Lapertot, D. Aoki, and L. P. Regnault
SPSMS, UMR-E CEA / UJF-Grenoble 1, INAC, 38054 Grenoble, France

A. Ivanov
Institut Laue Langevin, 38042 Grenoble, France

P. Piekarz and K. Parlinski
Institute of Nuclear Physics, Polish Academy of Sciences, 31-342 Krakòw, Poland

D. Legut
IT4Innovations Centre, VSB Technical University of Ostrava, Ostrava, Czech Republic

C. C. Homes
Condensed Matter Physics and Materials Science Department, Brookhaven National Laboratory, Upton, New York 11973, USA

P. Lejay
Institut Néel, CNRS et Université Joseph Fourier, BP166, F-38042 Grenoble Cedex 9, France

R. P. S. M. Lobo
LPEM, PSL Research University, ESPCI-ParisTech, 10 rue Vauquelin, F-75231 Paris Cedex 5, France;
CNRS, UMR 8213, F-75005 Paris, France;
and Sorbonne Universités, UPMC Univ Paris 06, F-75005 Paris, France
(Received 12 October 2014; published 26 January 2015)

We report a comprehensive investigation of the lattice dynamics of URu_2Si_2 as a function of temperature using Raman scattering, optical conductivity, and inelastic neutron scattering measurements as well as theoretical *ab initio* calculations. The main effects on the optical phonon modes are related to Kondo physics. The B_{1g} (Γ_3 symmetry) phonon mode slightly softens below ∼100 K, in connection with the previously reported softening of the elastic constant, C_{11}-C_{12}, of the same symmetry, both observations suggesting a B_{1g} symmetry-breaking instability in the Kondo regime. Through optical conductivity, we detect clear signatures of strong electron-phonon coupling, with temperature-dependent spectral weight and Fano line shape of some phonon modes. Surprisingly, the line shapes of two phonon modes, $E_u(1)$ and $A_{2u}(2)$, show opposite temperature dependencies. The $A_{2u}(2)$ mode loses its Fano shape below 150 K, whereas the $E_u(1)$ mode acquires it below 100 K, in the Kondo crossover regime. This may point to momentum-dependent Kondo physics. By inelastic neutron-scattering measurements we have drawn the full dispersion of the phonon modes between 300 and 2 K. No remarkable temperature dependence has been obtained, including through the hidden order transition. *Ab initio* calculations with the spin-orbit coupling are in good agreement with the data except for a few low-energy branches with propagation in the (a,b) plane.

DOI: 10.1103/PhysRevB.91.035129 PACS number(s): 71.27.+a, 63.20.dd, 78.30.Er, 78.70.Nx

I. INTRODUCTION

After almost three decades [1] of intensive experimental and theoretical research, the nature of the ordered phase found in the Kondo system URu_2Si_2 at temperature below $T_0 = 17.5$ K remains to be unraveled [2,3]. Whereas appearing clearly in the thermodynamic and transport quantities [1,4,5], the order parameter of this electronic hidden order (HO) state could not be determined by any usual or sophisticated experimental techniques [6]. Theoretical proposals are numerous, starting from itinerant or localized picture for the 5f electrons [7–16].

Particular features of the HO state have been determined. Inelastic neutron measurements [6,17,18] observe two magnetic excitations with a commensurate wave vector $Q_0 = (1,0,0)$ and an incommensurate wave vector $Q_1 = (1.4,0,0) \equiv (0.6,0,0)$, the first one being a fingerprint of the HO state [19]. A partial Fermi-surface gapping with a strong reduction of the carriers number occurs at T_0 [20,21]. At higher temperature, a heavy-electron Kondo liquid regime emerges below ∼100 K [1,22,23]. This cross-over temperature, observed in resistivity for instance, has been shown to be drastically reduced under high magnetic field [24] until the HO state vanishes at ∼35 T, suggesting that the Kondo liquid regime is a precursor of the HO state. It is well admitted that a Brillouin zone folding from a body center tetragonal (bct) to a simple tetragonal (st) phase occurs upon entering the HO state [16,25,26]. Recently,

*marie_aude.measson@univ-paris-diderot.fr

 ©2015 American Physical Society

various experiments have identified a fourfold symmetry breaking upon entering the HO state [27,28] and orthorhombic static lattice distortion has been reported by Tonegawa *et al.* [29].

The physics of URu_2Si_2 being mainly electronic, the lattice properties have been hardly investigated. Raman scattering [30] mainly reported temperature dependence of the intensity of the fully symmetric phonon mode, and optical conductivity studies were mostly focused on the electronic properties. A more detailed study by ultrasonic measurements versus temperature and under high magnetic field [31,32] reported a softening of the elastic constant C_{11}-C_{12} below $\sim$120 K, suggesting a B_{1g}-type (or Γ_3) lattice instability in connection with the Kondo crossover. Quite recently, an anomalous phonon softening below T_0 in the [1,1,0] direction has been reported by inelastic neutron scattering [33], calling for further detailed studies.

We report here a comprehensive study of the lattice dynamics of URu_2Si_2 from 300 to 2 K; the optical phonon modes have been investigated by Raman scattering (Sec. III) and infrared (IR) (Sec. IV) spectroscopies, the dispersion of the phonon branches by inelastic neutron scattering (including polarization techniques) (Sec. V), and *ab initio* calculations (Sec. VI) were used for comparison with all measurements.

II. PHONON MODES IN URu_2Si_2 AND SELECTION RULES

The URu_2Si_2 compound belongs to the tetragonal space group I4/mmm (D_{4h}), with the U, Ru, and Si atoms located at the 2a, 4d, and 4e Wyckoff positions, respectively. From group symmetry analysis [34], 8 zone center optical phonons are expected, A_{1g}, B_{1g}, $2E_g$, $2A_{2u}$, and $2E_u$. Due to inversion center in URu_2Si_2 elementary cell, the gerade (g) mode are Raman active and the ungerade (u) ones are IR actives. The corresponding atomic displacement patterns are sketched in Fig. 1. A_{1g} and B_{1g} modes involve motions of the Si and Ru atoms, respectively, along the c axis. The E_g modes correspond to the motions of Si and Ru atoms in the (a,b) plane. The IR active modes involve motions of all atoms along the c axis for the A_{2u} modes and in the (a,b) plane for the E_u modes.

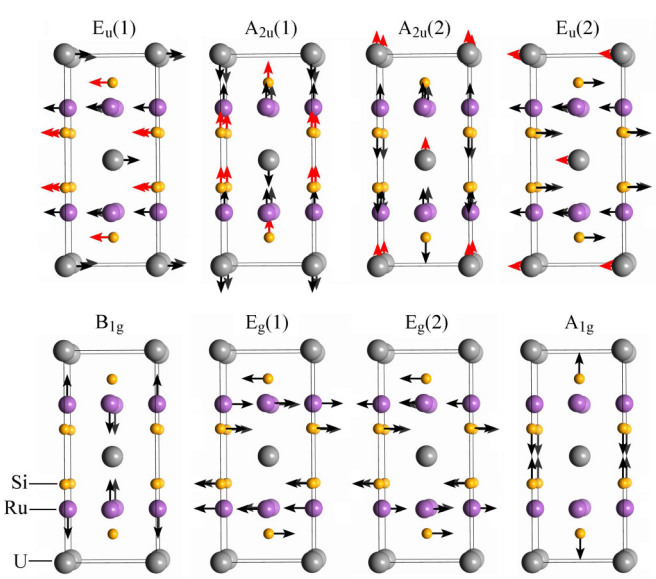

FIG. 1. (Color online) Atomic displacements sketches of the IR-active optical modes (up) and of the Raman-active optical modes (bottom) of URu_2Si_2. From left to right, the modes have increasing energy. The red arrows indicate the displacements with very low atomic intensities as calculated from *ab initio* studies (see Sec. VI).

In optical measurements, all the symmetries have been probed by combining different orientations of the samples and/or different incident ($\vec{e}_i$) and scattered ($\vec{e}_s$) light polarizations. Both Raman and IR scattering probes excitation with a transferred wave vector $\vec{Q}$ close to zero. To obtain the full dispersion of the optic and acoustic phonon branches we have carried out inelastic neutron scattering (INS). Here the transverse or longitudinal character of the phonon modes has been obtained by using different configurations of scattering vector $\vec{Q}$ as well as by comparison with the theoretical prediction for each branch.

III. RAMAN SPECTROSCOPY OF THE PHONONS

A. Methods

Polarized Raman scattering has been performed in quasi-backscattering geometry with an incident laser line at 532 nm from a solid state laser. We have used a closed-cycle ^{4}He cryostat with sample in high vacuum (10^{-6} mbar) for the measurements from 8 to 300 K and a ^{4}He pumped cryostat with the sample in exchange gas for measurements below 8 K or under magnetic field up to 10 T. By comparing Stokes and anti-Stokes Raman spectra and via the evolution of phonon frequencies with incident laser power, we have estimated the laser heating of the samples at +1.3 K/mW and +1 K/mW for the samples in high vacuum and in exchange gas, respectively. Typical laser power of 5 mW was used. The scattered light was analyzed by a Jobin Yvon T64000 triple substractive grating spectrometer equipped with a cooled CCD detector. In the triple substractive configuration we used, the resolution of the spectrometer is 2.5 cm^{-1}. For large energy-scale measurements (up to 3000 cm^{-1}), the spectrometer was used in the simple grating configuration. The contribution of the Bose factor has been removed for all spectra.

B. Sample preparation

The URu_2Si_2 single crystals were grown by the Czochralski method using a tetra-arc furnace [35]. The initial residual resistivity ratio of the samples is about 50. Two samples from the same batch, labeled 1 and 2, were polished along the (a,c) and (a,a) planes, respectively. By cleaving, we obtained samples along the (a,a) plane. The E_g phonon modes can be probed only in (a,c) plane [$\vec{E}//(a,c)$], so only on polished sample. Figure 2 shows the A_{1g} and B_{1g} phonon modes after polishing then after annealing, for samples 1 and 2 (see inset). After polishing along the (a,c) plane (sample 1), both phonon modes are shifted by about 4% to higher energy and broadened. Most probably, the stress induced by polishing gives rise to such hardening and to the shortening of their lifetime. However, no such stress effect has been observed on the sample polishing along (a,a) plane (see inset of Fig. 2). In order to release the stress induced by polishing, both samples have been annealed for two days at 950° under ultra-high

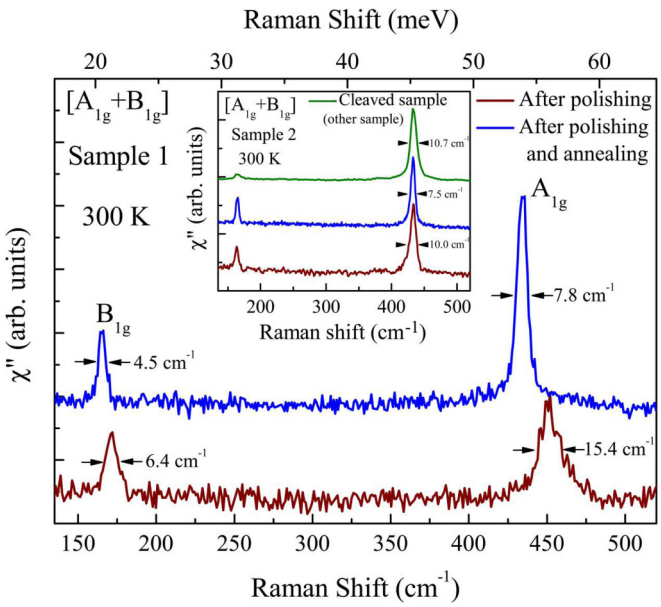

FIG. 2. (Color online) Raman spectra of URu_2Si_2 for sample 1 after polishing along the (a,c) plane and annealing. Inset: Raman spectra for sample 2 after polishing along the (a,a) plane, annealing, and for another sample cleaved along the (a,a) plane.

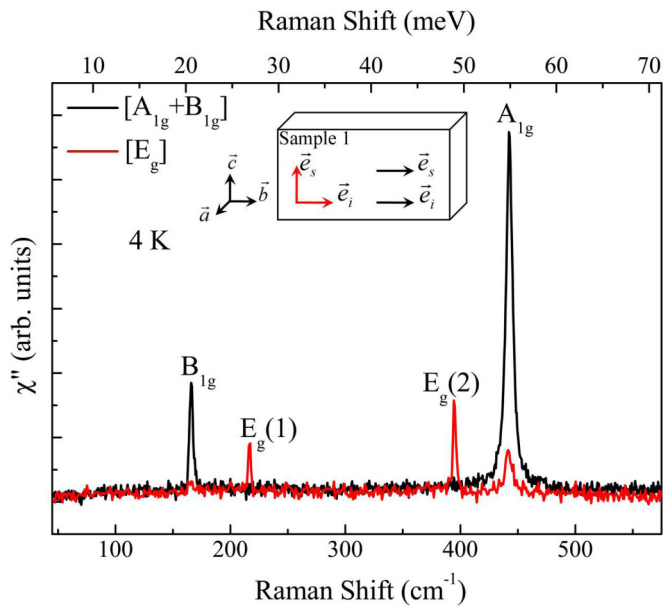

FIG. 3. (Color online) Typical Raman spectra measured at 4 K in cross- and parallel-polarization of the light. A scheme of sample 1 with the orientation of the polarizations of the incident $\vec{e}_i$ and scattering $\vec{e}_s$ light is shown.

vacuum. This process has shifted down the phonon modes and it has clearly sharpened them. The final position and width are similar to what is measured on the cleaved sample of the same batch [36] (see inset of Fig. 2). (Note that even sharper A_{1g} phonon mode with a full width at half maximum (FWHM) at 4 K of 4 cm^{-1} have been measured on cleaved samples from another batch.) The E_g modes measured on final sample 1 are very sharp, comparable to the resolution of the spectrometer at low temperature.

C. Results and Discussion

Figure 3 shows typical Raman spectra obtained at 4 K on sample 1 after polishing and annealing. A_{1g} and B_{1g} phonon modes are visible in parallel polarization and E_g modes in cross-polarization. We observe a leakage of the A_{1g} mode in cross-polarization due to a weak crystal misalignment. At 300 K, the two E_g modes are seen at 213 and 391 cm^{-1}, and A_{1g} and B_{1g} at, respectively, 434 and 163 cm^{-1}. The B_{1g} and both E_g phonon modes are sharper (with a FWHM of 3.2 cm^{-1}, 2.8 cm^{-1}, and 1.8 cm^{-1} at 4 K, respectively) than the A_{1g} phonon mode (FWHM = 6.6 cm^{-1} at 4 K). All phonons have a Lorentzian line shape.

Figures 4 and 5 present the temperature dependence of the energies and FWHM of the Raman-active phonon modes. The energies are normalized to their value at 300 K. We have investigated precisely the energy of the phonons through the hidden order transition but no particular effect has been observed within our accuracy (See inset of Fig. 4). The energy of the A_{1g} mode increases with decreasing temperature before saturating at 1.25% higher energy than at 300 K. It narrows upon cooling before saturating. The general temperature dependence of this mode is naturally explained by anharmonic effects [37,38]. Other ingredients, like anharmonic effect of higher rank (four-phonon process), would be necessary to accurately fit the data.

The temperature dependence of the A_{1g} mode energy is consistent with previous Raman experiments [39]. No particular change of the integrated intensity of the A_{1g} phonon mode has been detected contrary to what Cooper *et al.* have reported [39]. Nor do we see any abrupt increase of the

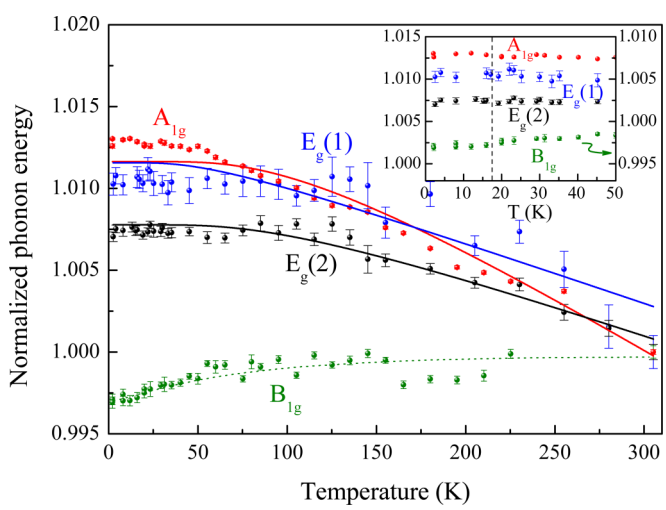

FIG. 4. (Color online) Temperature dependence of the position of the A_{1g}, $E_g(1)$, $E_g(2)$, and B_{1g} phonon modes normalized to their value at 300 K. B_{1g} phonon exhibits an unusual softening when cooling down below 100 K. Error bars have been extracted from the Lorentzian fits. Lines are fits with a single anharmonic model [37,38]. The green dot line is a guide to the eyes. Inset: zoom of the data at low temperature (hidden order transition is marked by the vertical black dashed line). No particular anomaly is measured at T_0.

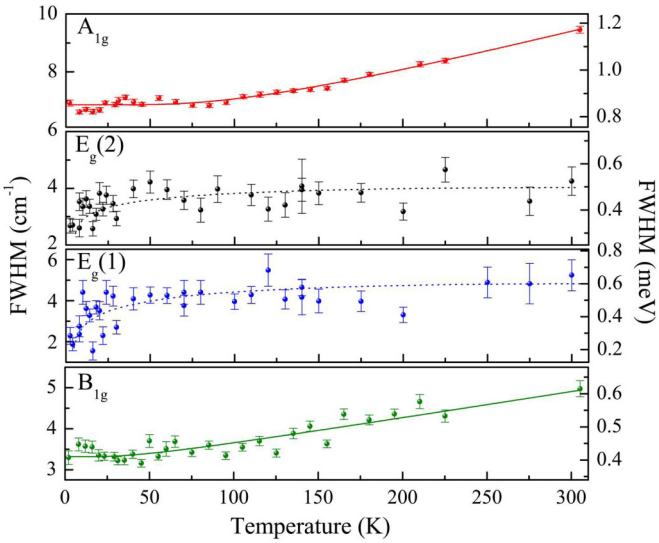

FIG. 5. (Color online) Temperature dependence of the FWHM of A_{1g}, $E_g(1)$, $E_g(2)$, and B_{1g} phonon modes. Lines are fits with a single anharmonic model [37,38]. Dot lines are guides to the eyes.

linewidth of A_{1g} below 20 K contrary to what is reported by Lampakis *et al.* [40].

Whereas both E_g modes exhibit usual increasing energy when cooling down, their FWHM are almost constant in all the temperature range. A slight sharpening seems to appear below 20–30 K, which might be concomitant with the electronic gap opening at T_0 observed by optical conductivity [20,41–43] and Raman scattering [26].

Intriguingly, whereas the FWHM of the B_{1g} phonon shows the usual temperature evolution with narrowing when temperature decreases, its energy remains constant down to about 100 K before softening by about 0.5% below. This softening occurs in the temperature range of the Kondo cross-over and upon entering the Kondo liquid regime below the Kondo temperature reported between 70 K [1,22] and 120 K [23]. Clearly, the temperature dependence of the energy of the B_{1g} phonon cannot be reproduced by the simple anharmonic model. This behavior indicates possible electron-phonon interactions not included in this simple model and involving electronic states not only close to the Fermi surface but from much larger energy range.

Finally, we have probed all phononic excitations under high magnetic field up to 10 T (not shown). No effect has been observed.

The unusual temperature dependence with softening below the Kondo temperature of the energy of the fourfold rotational symmetry breaking B_{1g} phonon mode suggests a tendency toward lattice instability with orthorhombic distortion. Fourfold symmetry breaking and even orthorhombic distortion upon entering the HO state have been reported by various experiments [27–29]. However, the symmetry broken here is B_{2g}, i.e., 45° from the B_{1g} symmetry, both being in the (a,b) plane. Clearly, there is no direct relationship between these measurements and our Raman scattering result. The tendency toward lattice instability with B_{1g} symmetry is most probably related with the Kondo physics. Interestingly, similar softening effect (of 0.7%) of the elastic constant $(C_{11}\text{-}C_{12})/2$ in the same symmetry ($B_{1g} \equiv \Gamma_3$) has been reported below 120 K by ultrasound velocity measurements [31]. In addition, they show that this effect disappears when high magnetic field of 35 T is applied along the c axis. At this magnetic field, the coherence temperatures are strongly reduced concomitantly with the vanishing of the hidden order phase [24]. The softening of the elastic constant $(C_{11}\text{-}C_{12})/2$ has been related to the emergence of the hybridized electronic state between the $5f$ electron and the conduction electrons (s or d) and associated to a symmetry-breaking band instability. Both results, on acoustic (ultrasound experiment) and optical phonon (Raman experiment) modes, are nicely consistent and point to a B_{1g} symmetry-breaking instability upon entering into the Kondo regime of URu_2Si_2. While the acoustic phonon modes involve the motion of all atoms, the B_{1g} mode involves only the Ru atoms. This may suggest that the electronic environment of the Ru atoms are particularly affected by the Kondo physics.

On the basis of our inelastic neutron scattering study and theoretical calculations, two origins for this small B_{1g} lattice instability are unlikely. First, our theoretical calculations including global anharmonic effects from purely phononic origin (See Sec. VI and Fig. 14) indicates that none of the phonon branches, except the A_{2u} one, are strongly affected by these anharmonic effects. Second, by following the full dispersion of the "B_{1g}" branch as well as magnetic excitations by inelastic neutron scattering (see Sec. V) we show that the k-dependence of the phonon is smooth going through the minima in the magnetic dispersion ($\vec{Q}_0$ and $\vec{Q}_1$). This does not give any indication of magnetoelastic coupling. Finally, as the B_{1g} mode is not affected by the large loss of carriers upon entering the HO state, as the phenomenon which induces the unusual B_{1g} energy behavior does not involve any noticeable change of its FWHM, an electron-phonon coupling involving electronic states from the broad range of energies and influenced by the Kondo physics is certainly in play for this B_{1g} mode.

IV. OPTICAL CONDUCTIVITY OF PHONONS

A. Methods

Unpolarized optical reflectivity was measured on a cleaved $2 \times 3\text{-mm}^2$ (a,a) plane on Bruker IFS66v and IFS113v interferometers. The c axis reflectivity was taken with appropriate polarizers on sample 1 (see Sec. III), an optically polished $1 \times 1.5\text{-mm}^2$ (a,c) surface. We verified that unpolarized data on the (a,a) plane at 5 K was identical to a-polarized measurements on the (a,c) surface. Spectra were recorded at several temperatures from 5 to 300 K, between 20 cm^{-1} (2.5 meV) and 12 000 cm^{-1} (1.5 eV). This data was extended to 40 000 cm^{-1} (5 eV) at room temperature in a AvaSpec-2048x14 grating fiber spectrometer. To obtain the absolute reflectivity we utilized an *in situ* overfilling (gold or aluminum) evaporation technique [44]. For Kramers-Kronig analysis, we took a Hagen-Rubens extrapolation below our lowest measured frequency. Above 40 000 cm^{-1}, we utilized the data by Degiorgi *et al.* [45] up to 100 000 cm^{-1} (12 eV), followed by a ω^{-4} free electron termination.

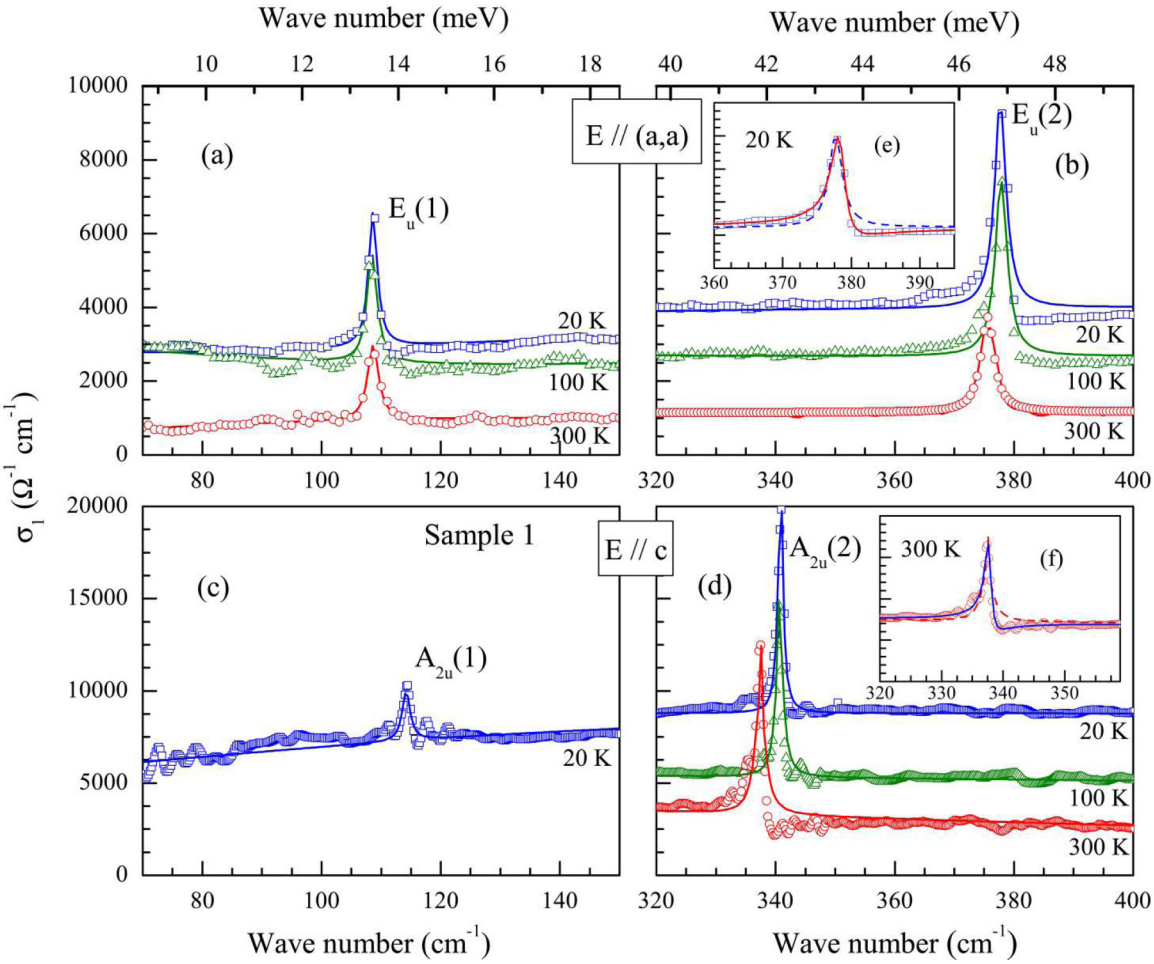

FIG. 6. (Color online) Optical conductivity centered around each phonon of URu_2Si_2 at selected temperatures. Panels (a) and (b) are for light polarized on the (a,a) plane, and panels (c) and (d) are for measurements along the c direction. Symbols are the data and the lines are Drude-Lorentz fits as described in the text. Inset (e) shows the highest frequency $E_u(2)$ mode at 20 K described by either a Lorentz oscillator (dashed line) or a Fano mode (solid line). Panel (f) is the equivalent to panel (e) for the highest frequency $A_{2u}(2)$ mode at 300 K.

B. Results and Discussion

Figure 6 shows the optical conductivity around each phonon for both polarizations. We do observe all predicted modes by group theory: 2 E_u phonons in the (a,a) plane [Figs. 6(a) and 6(b)] and 2 A_{2u} modes along the c direction [Figs. 6(c) and 6(d)]. This is the first observation of the very weak A_{2u} phonon at 115 cm^{-1}, which we could only detect at low temperatures. Above ~30 K, this phonon becomes too broad to be resolved in the spectra. Small wiggles in the spectra are experimental artifacts.

In Figs. 6(a)–6(d) the symbols are the data and the solid lines are fits utilizing a Drude-Lorentz approach. We accounted for the continuum with one Drude peak and two broad Lorentz oscillators. This is a convenient way to parametrize the data but the values of the parameters do not carry a particular physical meaning. On top of this continuum we added a Lorentz oscillator for each phonon. One can see that the Lorentz oscillator describes reasonably well the phonon responses although the line shape is not perfect at a few temperatures, such as 20 K in Fig. 6(b) and 300 K in Fig. 6(d) (Fano line shapes will be discussed later). Nevertheless, the Lorentz oscillator is very useful in analyzing the phonon spectral weight.

The spectral weight, characterizing the charge in a restricted spectral range, is defined as an integral over the real part of the optical conductivity σ_1:

$$S_a^b = \int_{\omega_a}^{\omega_b} \sigma_1(\omega)\, d\omega\,. \tag{1}$$

When $\omega_a \to 0$ and $\omega_b \to \infty$, one recovers the f-sum rule $S = (\pi/2)(ne^2/m)$ (n is the total number of electrons, e is the electronic charge, and m the bare electronic mass). This rule states that the total integral under the real part of the optical conductivity is a constant independent of external parameters such as the temperature or pressure.

The spectral weight for a phonon within the Lorentz framework is

$$S_p = \frac{\pi^2}{Z_0}\omega_p^2\,, \tag{2}$$

where Z_0 is the vacuum impedance, and ω_p is the phonon plasma frequency. If phonons were decoupled from each other and from other excitations (e.g., electronic continuum), Eq. (2) should be temperature independent for each phonon.

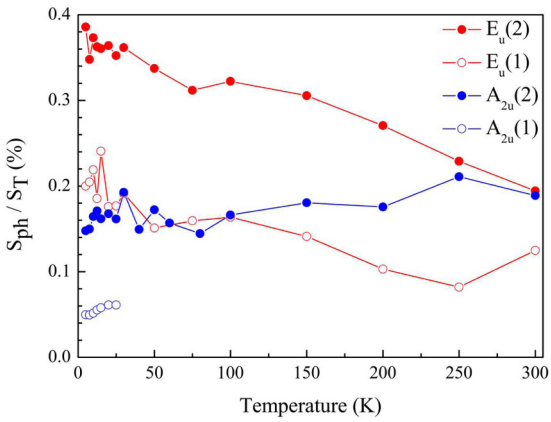

FIG. 7. (Color online) Spectral weight of each phonon normalized by the spectral weight up to 2 000 cm^{-1} calculated at room temperature.

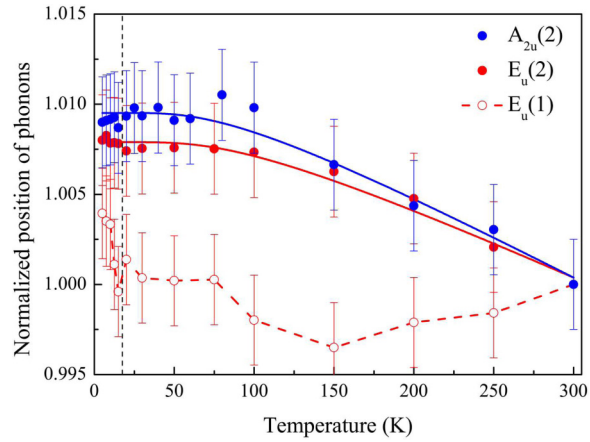

FIG. 8. (Color online) Temperature dependence of the frequency of $A_{2u}(2)$, $E_u(1)$, and $E_u(2)$ phonon modes normalized to their value at 300 K. Lines are fits with a single anharmonic model (see Sec. III C). The vertical black dashed line marks the transition into the hidden order.

Figure 7 shows the temperature dependence of the spectral weight of each phonon from Eq. (2), normalized by the total spectral weight (integrated up to 2 000 cm^{-1}) for its respective polarization at room temperature. Data for the lowest-frequency A_{2u} is shown for completeness, but we do not have enough temperatures to draw any conclusion about this phonon.

The spectral weight of both E_u phonons almost doubles upon cooling the sample from room temperature to 5 K. The highest-energy A_{2u} phonon also shows a temperature-dependent spectral weight, albeit of smaller magnitude. Interestingly, for this phonon, the spectral weight decreases with decreasing temperature.

This behavior indicates that the effective charge of the phonons change with temperature. As the sum rule states that the total spectral weight must be conserved, this charge must be transferred from or to some other excitation. Because the spectral weight of the phonons correspond to less than 1% of the total spectral weight, we do not have enough resolution to pinpoint the energy (and hence the excitation) from which this charge is being transferred. However, the obvious candidate is the electronic continuum.

Indeed, let us go back to Fig. 6 and make a closer inspection on the phonon line shapes. The asymmetric line shapes observed cannot be described by a Lorentz oscillator. Indeed, The Lorentz model does not take into account coupling between localized (e.g., phonon) states and the continuum. Fano [46] described phonon line shapes when an electron-phonon coupling exists. Here we adopt the formalism proposed by Davis and Feldkamp [47], who generalized Fano's approach to multiple discrete states:

$$\sigma_1^F = \frac{2\pi}{Z_0} R\omega \left\{ \frac{[q\gamma + (\omega - \Omega)]^2}{\gamma^2 + (\omega - \Omega)^2} - 1 \right\}, \qquad (3)$$

where Ω and γ are the phonon resonance frequency and width, respectively. R is a renormalization parameter that takes into account the transition rate between continuum and localized states. The important parameter in our analysis is the Fano-Breit-Wigner q^{-2}, which vanishes when the electron-phonon interaction disappears. It probes the continuum density of states at the phonon frequency.

In Fig. 6(e), we show the data for the highest E_{2u} phonon fitted by either a Lorentz oscillator (dashed line) or a Fano mode (solid line) at 20 K. Only the latter properly describes the asymmetry observed in the measured data. This is the hallmark of an electron-phonon coupling and substantiates our claim that the phonon charge is changing due to a spectral weight transfer with the electronic continuum. Figure 6(f) shows that the same effect is present in the highest energy A_{2u} mode at 300 K.

From our Fano mode fitting, we extracted the temperature dependence of the phonons energy normalized to their value at 300 K as presented Fig. 8. At 300 K, the two E_u phonon modes are seen at 108.7 and 375.6 cm^{-1}, and the highest A_{2u} phonon mode at 337.8 cm^{-1}. Whereas the $E_u(2)$ and $A_{2u}(2)$ phonon modes exhibit the expected hardening when cooling down, the $E_u(1)$ phonon mode shows constant energy down to ~20 K and a small hardening of ~0.2% upon entering the HO phase. Even if only this low-energy phonon $E_u(1)$ has a singular temperature dependence, the $E_u(2)$ and $A_{2u}(2)$ phonon modes exhibit Fano line shapes with peculiar temperature dependencies, again evidencing that a complex electron-phonon coupling is in play in URu_2Si_2.

Figure 9 shows the temperature behavior for the Fano-Wigner-Breit parameter for both E_u [(1) at 108 cm^{-1} and (2) at 378 cm^{-1}] and the highest-energy $A_{2u}(2)$ (at 340 cm^{-1}) phonons. The q^{-2} parameter for mode $E_u(2)$ shows a behavior similar to its effective charge. Both quantities increase almost featurelessly with decreasing temperature. This joint behavior corroborates the electron-phonon coupling for this mode. Whereas mode E_u shows a clear drop in q^{-2} at T_0, directly related to the loss of carriers number at the hidden order transition, we cannot pinpoint a particular change of coupling in the paramagnetic state.

Phonons $E_u(1)$ and $A_{2u}(2)$, on the other hand, show a striking change of regime close to the Kondo transition where

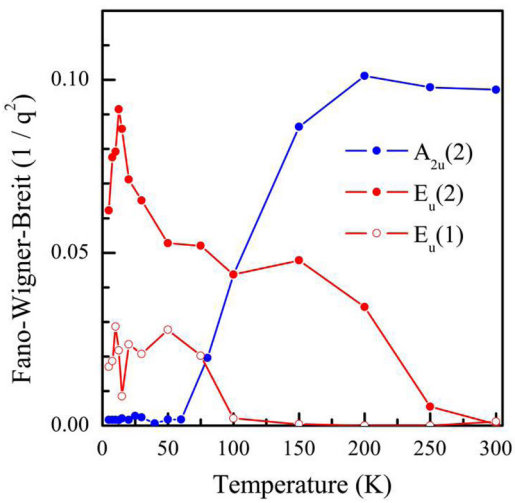

FIG. 9. (Color online) Temperature dependence of Fano-Wigner-Breit q^{-2} parameter for both E_u and the highest frequency A_{2u} phonons. When an electron-phonon coupling occurs, the Fano-Wigner-Breit q^{-2} parameter becomes different from zero.

coherent transport develops. $E_u(1)$ has a very small, yet finite, q^{-2} at high temperatures. Close to the Kondo temperature it suddenly increases and the phonon develops an asymmetric shape. The opposite is observed for phonon $A_{2u}(2)$, which has an asymmetric shape and a large q^{-2} value above the Kondo temperature.

The temperature dependence of q^{-2} probes the variation of the continuum density of states close to the phonon energy. A decrease in q^{-2} indicates a gap (or at least a depletion) on the density of states close to the phonon energy. Along these lines, the behavior of the A_{2u} mode suggests that we would have a gapped system along k_z around 40 meV in the Kondo regime. Phonon $E_u(1)$, conversely, hints that the system is gapped or with a strongly depleted density of states on the (k_x,k_y) plane at about 12 meV but this gap closes below the Kondo temperature or more generally the electronic density of state is enhanced when entering into the Kondo liquid regime.

Such observation of a temperature-dependent Fano shape of a phonon mode in metallic Kondo systems has already been reported in $CeCoIn_5$ by Raman scattering [48]. Indeed, according to their study of the lattice dynamics and electronic Raman response of $CeCoIn_5$, the entrance into the Kondo liquid regime below the crossover temperature $T^* \sim 45$ K manifests itself by the divergence of the Fano coefficient of the A_{1g} phonon and by the significant drop of the scattering rate of the electronic scattering background. Both have been related to the enhancement of the electronic density of states due to the hybridization of $4f$ electrons with the conduction band. However, the behavior as measured on the $A_{2u}(2)$ mode in URu_2Si_2 and even more the concomitant opposite behaviors of two phonons $A_{2u}(2)$ and $E_u(1)$ within the same compounds is striking and has never been reported to our knowledge. Most probably, this points to strongly momentum-dependent Kondo physics in URu_2Si_2, which affect distinctively both phonon modes with movements into different and perpendicular planes, namely the (x,y) and (z) planes.

V. PHONONS AND MAGNETIC EXCITATIONS STUDIES BY INELASTIC NEUTRON SCATTERING

A. Methods

The phonon spectrum of URu_2Si_2 was investigated by inelastic neutron scattering (INS) at the Institute Laue-Langevin. The first experiment was performed on the thermal neutron three-axis spectrometer IN8. In the first configuration, the initial beam is provided by a double focusing Si monochromator [Si(1,1,1)] and the scattered beam is analyzed by a double focusing pyrolytic graphite (PG) analyzer [PG(0,0,2)] with fixed $k_F = 2.662$ Å^{-1}. In the second configuration, the initial beam is provided by a double-focusing Cu monochromator [Cu(2,0,0)] and the scattered beam is analyzed as previously but with fixed $k_F = 4.1$ Å^{-1}. This second configuration is used to investigate high-energy modes. The second experiment was performed on the thermal neutron three-axis spectrometer IN22, where the initial beam is provided by a double-focusing PG monochromator [PG(0,0,2)] and the scattered beam is analyzed by a double-focusing PG analyzer [PG(0,0,2)] with fixed $k_F = 2.662$ Å^{-1}. For these two experiments, the sample is a cylinder of diameter 4.5 mm and of length 8 mm along the a axis; the scattering plane is defined by (1,0,0) and (0,0,1). The third experiment was performed on IN22 in polarized neutron setup with Heussler monochromator and analyzer with fixed $k_F = 2.662$ Å^{-1}. The neutron polarization is kept along the neutron path by guide fields and by an Helmholtz coil around the sample; a Mezei flipper is placed before the analyzer. The experiment was performed with the neutron polarization parallel to the scattering vector (**P//Q**). With this configuration, all the magnetic scattering appears in the spin-flip (SF) channel while the phonon scattering appears in the non-spin-flip (NSF) channel. For this experiment, the sample is a cylinder of diameter 4.5 mm and of length 12 mm along the c axis, and the scattering plane is defined by (1,0,0) and (0,1,0). In all the measurements, the sample was inside an helium-4 flow cryostat covering the range 2–300 K. A PG filter was always placed in the scattered beam in order to remove higher-order contamination. (Note for comparison between Raman, IR, and neutron scattering that 1 meV = 8.06 cm^{-1}). The data were fitted without taking into account the resolution effect. Damped harmonic oscillator line shape and ω-lorentzian line shape [49] functions were used to fit the phonons and the magnetic excitations, respectively.

B. Results and Discussion

In the present paper, the scattering vector **Q** is decomposed into $\mathbf{Q} = \mathbf{G} + \mathbf{q}$, where **G** is a reciprocal lattice wave vector and **q** is the wave-vector of the excitation. The cartesian coordinates of $\mathbf{q} = (h, k, l)$ are expressed in reciprocal lattice units (r.l.u.). Representative phonon spectra measured on IN8 are shown in Fig. 10(a) for $\mathbf{Q} = (0, 0, 5.25)$. The two peaks at 11.8 and, respectively, 17.5 meV correspond to longitudinal acoustic (LA) and, respectively, longitudinal optic (LO) modes. The data at 2 and 60 K are described by using the parameters obtained at 300 K, except the intensity that is rescaled by the temperature population factor. This procedure allows us to spot anomalous temperature behavior of the phonons.

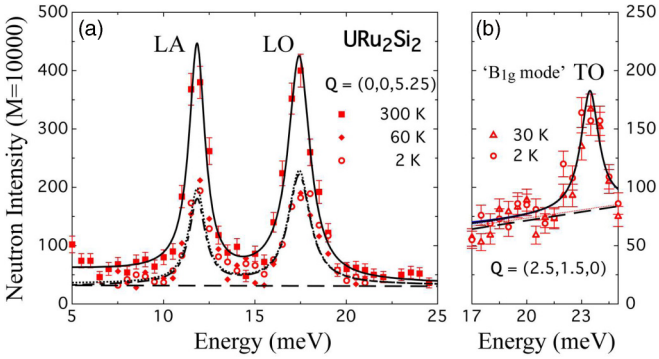

FIG. 10. (Color online) Inelastic neutron scattering phonon spectra measured for (a) $\mathbf{Q} = (0, 0, 5.25)$ at $T = 2$, 60, and 300 K performed on IN8, and (b) $\mathbf{Q} = (2.5,1.5,0)$ at $T = 2$ and 30 K performed on IN22. L and T, A and O stand for longitudinal and transverse, acoustic and optic, respectively. The TO mode belongs to the branch that corresponds to the B_{1g} mode at $\mathbf{Q} = 0$. Lines are fits of the data with an harmonic oscillator line shape and sloppy background. The neutron intensity is given for a normalized incident flux (M), which corresponds to a counting time of approximately 80 s.

The overall phonon modes measured along [0, 0,1], [1,0,0], and [1,1,0] directions do not show noticeable temperature dependence on cooling from 300 to 2 K or on crossing T_0, except for a small expected hardening (see the LO branch in Fig. 10 shifting a little to higher energy with decreasing temperature), which is a normal behavior of phonon on cooling. Although the softening of the B_{1g} mode seen by Raman scattering is too small (0.5%) to be detected by neutron measurement, a larger softening could occur at finite $\mathbf{q}$. Therefore, a particular attention has been focused on the temperature dependence of the "B_{1g}" branch for $\mathbf{q} \neq 0$ in [0, 0,1] and [1,1,0] directions. As presented, for instance, in Fig. 10(b) for $\vec{Q} = (2.5,1.5,0)$, no temperature difference has been observed between 2 K and 30 K.

Figure 11 shows the four phonon modes E_u, E_g, A_{2u}, and A_{1g} seen at Γ point by INS. A good agreement is found with the energy of these phonon modes measured by IR and Raman spectroscopy.

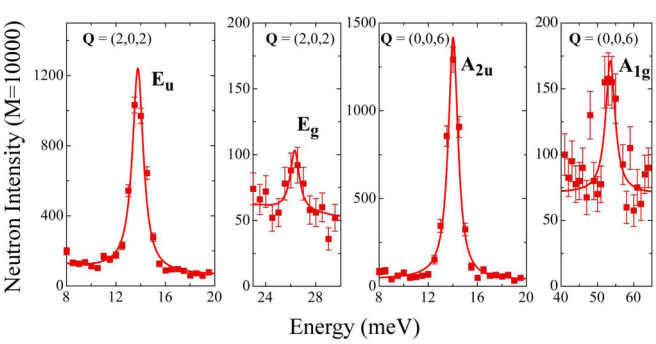

FIG. 11. (Color online) Inelastic neutron scattering phonon spectra at Γ point measured for $\mathbf{Q} = (2, 0, 2)$ and $\mathbf{Q} = (0, 0, 6)$ at $T = 300$ K. The E_u and E_g phonon modes have been observed for $\mathbf{Q} = (2, 0, 2)$ and A_{2u} and A_{1g} phonon modes for $\mathbf{Q} = (0, 0, 6)$. The neutron intensity is given for a normalized incident flux (M), which corresponds to a counting time of approximately 80 s for E_u, E_g, A_{2u} and 110 s for A_{1g}. Lines are fits of the data with an harmonic oscillator line shape.

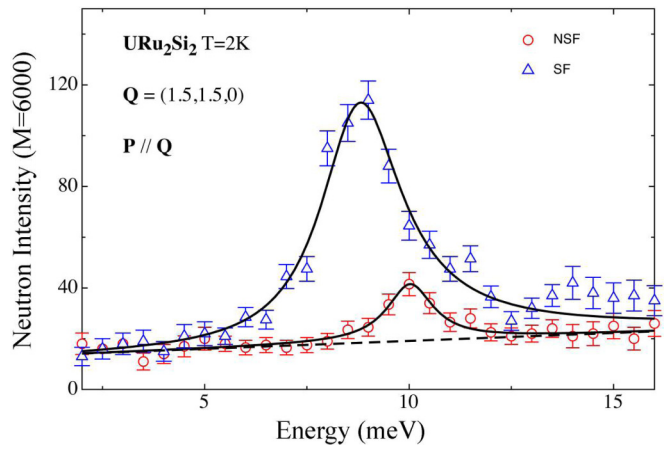

FIG. 12. (Color online) Polarized inelastic neutron scattering spectra measured for $\mathbf{Q} = (1.5, 1.5, 0)$ in the non-spin-flip (NSF) and spin-flip (SF) channels for $T = 2$ K. Full lines are fits of the data with functions described in the text. The dashed line indicates the background. The neutron intensity is given for a normalized incident flux, which corresponds to a counting time (M) of approximately 25 min.

Further emphasis was given in the study of the phonons along the [1,1,0] direction by polarized neutron scattering following the report of anomalous phonon softening in this direction below T_0 [33]. Figure 12 shows a representative measurement performed on IN22, with the neutron polarization parallel to $\mathbf{Q}$, at X point in the Brillouin zone (see Fig. 13) for $\mathbf{Q} = (1.5, 1.5, 0)$ at $T = 2$ K for SF and NSF scattering. In the NSF scattering a phonon mode is observed at around 10 meV. In the SF channel, the large intensity peak centered at around 8.7 meV corresponds to the well-known magnetic excitation of URu_2Si_2. The peak position is in agreement with an early study performed along the [1,1,0] direction by Broholm *et al.* [6]. We therefore conclude the reported soft phonon mode [33] is in fact a magnetic excitation, an unambiguous result obtained by polarized INS [50].[1]

[1]After acceptance of our manuscript entitled "Lattice dynamics of the heavy fermion compound URu_2Si_2" for publication in Physical Review B, we were aware of a completed parallel study by N. P. Butch *et al.* of the lattice and magnetic excitations in URu_2Si_2 [50]. The magnetic nature of the excitations along ΓX below 10 meV is confirmed by their polarized neutron scattering measurement, which agrees with ours. Regarding the dispersion of the phonons, our studies are mostly consistent, including the absence of strong magnetoelastic coupling or any effect of orthorombic distortion, but differ concerning several details of temperature dependencies. Indeed, they report an inversion of the branches along the $\Gamma\Sigma Z$ direction. In this region, we measure the TO_1 branch at the same energy of 13.8 meV at 300 and 2 K, whereas the authors report a change of ~ 2 meV. We measured the energy of the LO_1 branch along the ΓZ direction at the position of their reported minimum: it is found to be at the same energy of 14.3 meV at 300, 60, and 2 K. We cannot comment on the LO_2 branch along ΓZ as we did not detect it. Finally, at the Z point, we measure no change in energy of the TA branch between 300 and 2 K. It is the same energy of 9.8 meV.

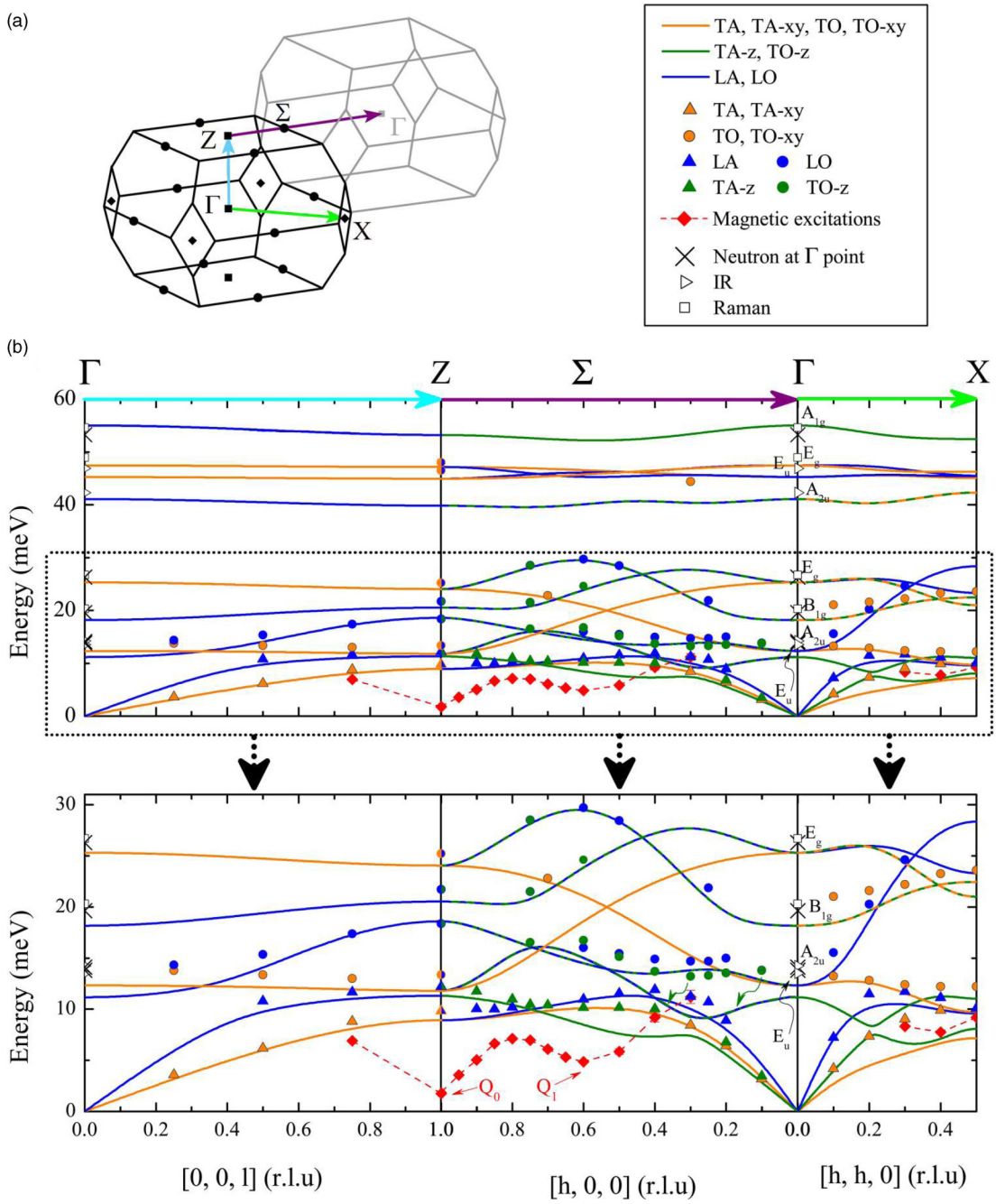

FIG. 13. (Color online) (a) Brillouin zone of the body-centered tetragonal crystal structure of URu_2Si_2 in the paramagnetic state. The arrows indicate the direction of the dispersion for the inelastic neutron scattering (INS) measurements, as reported below. (b) Phonons and magnetic excitations (full red diamonds) dispersion along the ΓZ ([0,0,1]), ZΣΓ ([1,0,0]), and ΓX ([1,1,0]) directions. Full circles and full upward triangles are INS data for the optical and acoustic branches, respectively. Each reported energy is the energy average of all measured temperature for each phonon mode (see text). Empty symbols are data obtained in the zone center at Γ, with cross, open triangles, and squares for INS, IR, and Raman measurements, respectively. Dashed lines are guides to the eyes for the magnetic excitations dispersion. Solid lines corresponds to the *ab initio* GGA calculation with spin-orbit coupling and $u = 0.06$ Å (see Sec. VI). When the dispersion curve has a mixed character (for instance from LO (in Γ) to TO-z (in Z) along [1,0,0]), the solid lines are bicolored. The black arrow points to the $E_u(1)$ phonon mode measured by IR at Γ point. The green arrows indicate the calculated branch, which corresponds to the measured points (green full circles). Q_0 and Q_1 correspond to the minima in magnetic excitation dispersion, known as commensurate and incommensurate excitations, respectively.

Figure 13 summarize all the phonon and magnetic excitations dispersions we have measured along the main directions [1,0,0], [0, 0,1], and [1,1,0]. As the error on the fitted energy of each phonon mode is about 1% and as we have not observed any variation of the phonon energies higher than 1% from 300 to 2 K, we have reported the energy average of all measured temperature for each phonon mode. There is a fairly good agreement between the measurement and the calculation,

TABLE I. Phonon energies, E, for the phonon modes of URu_2Si_2 in cm^{-1} at the Γ point obtained by Raman, infrared, and inelastic neutron-scattering measurements at the lowest temperature and by *ab initio* studies at 0 K. We report the energies calculated with the spin-orbit coupling and $u = 0.06$Å. The ones calculated without the spin-orbit coupling and with $u = 0.06$ Å are presented in parentheses. On the right: calculated atomic intensities of URu_2Si_2 with spin-orbit coupling and displacements of $u = 0.06$ Å for the lattice modes at the Γ point.

Phonon modes at Γ point	E measured by			E calculated	Atomic intensities		
	Raman spectroscopy	IR	neutron		U	Ru	Si
A_{2u}	–	114.8	111.2	90.1(84.7)	0.52	0.42	0.06
E_u	–	109.1	113.6	99.5(101.6)	0.52	0.42	0.06
B_{1g}	163.6	–	158.1(leakage)	146.7(144.2)	0	1.00	0.00
E_g	215.1	–	212.0	204.3(206.6)	0	0.74	0.26
A_{2u}	–	340.8	–	331.5(331.3)	0	0.17	0.83
E_u	–	378.6	–	365.3(364.2)	0	0.17	0.83
E_g	394.1	–	–	382.9(382.7)	0	0.26	0.74
A_{1g}	439.7	–	429.1	443.9(459.7)	0	0.00	1.00

which includes the spin-orbit coupling (see Sec. VI), except for few branches. The energy of the transverse (T) modes TA-z and TO-z (or "$A_{2u}(1)$" branch) along [1,0,0] and TA-xy along [1,1,0] lines is ∼20% higher than what is expected by the calculation.

We have not observed any magnetic excitations along [1,0,0] nearby Γ point. Then, most probably, the excitations reported by Broholm [6] in this $\vec{k}$-space zone are the optical phonon mode ("E_u" or "A_{2u}" branches).

Furthermore, we report no particular anomaly of the phonon branches around Q_0 and Q_1 points where magnetic excitations are centered. No strong magnetoelastic coupling related to these magnetic modes is in play in URu_2Si_2.

VI. THEORETICAL CALCULATIONS OF PHONON DISPERSION CURVES

A. Methods

The calculations have been performed using the density functional theory (DFT) implemented in the VASP software [51]. The electron potentials and wave functions were obtained within the projector-augmented waves method [52] and the exchange and correlation energy was described by the generalized-gradient approximation [53]. The expansion of the single-particle plane waves has been restricted by the energy cutoff of 340 eV. The electronic and crystal structure have been optimized in the $2 \times 2 \times 1$ supercell (40 atoms) with the periodic boundary conditions. We performed two types of calculations, with and without spin-orbit coupling (SOC), assuming in both cases the nonmagnetic ground state. The optimized lattice parameters show good agreement with the experimental values and the previous relativistic full-potential calculations [54].

The phonon dispersion curves were obtained by using the direct method [55,56]. In this approach, the force constants are derived from the Hellmann-Feynman (HF) forces calculated *ab initio* by displacing atoms from equilibrium positions. Due to symmetry constraints, only three atoms (Si, Ru, and U) have to be displaced along two nonequivalent directions, x and z. The phonon dispersions were calculated by the exact diagonalization of the dynamical matrix, obtained directly from the force constants.

B. Results and Discussion

The nature of the Raman and infrared-active vibrations as described by group theory is completed by a detailed description of the actual atomic character of the vibrations thanks to *ab initio* calculations of the phonon dispersion curves. The atomic intensities for each phonon branch at the Γ point is shown in Table I. In this case, the intensity refers to the square of the vibrational amplitude of each atom for a given branch. This is particularly useful for the infrared-active A_{2u} and E_u modes, which in principle involve displacements of all of the atoms in the unit cell. The atomic intensity reveals that at the Γ point, the low-frequency A_{2u} and E_u modes involve mainly the U and Ru atoms, while the high-frequency A_{2u} and E_u modes are almost entirely Si in character with a slight involvement of the Ru atom (cf. Fig. 1).

In order to investigate possible anharmonic effects, two different sets of displacements, with $u = 0.03$ Å and $u = 0.06$ Å, were used to derive the HF forces. This approach would give us information about the possible deviation from the harmonic potential and it has been used previously to study the anharmonic behavior in magnetite [57]. The results of both calculations are presented in Fig. 14. Instead of phonon softening typical for an anharmonic potential, we observe the increase in energy at larger value of u. The effect is more apparent for the TA-z and the lowest TO mode along the ΓX and $\Gamma \Sigma Z$ directions and TA-xy along the ΓZ direction. At the Γ point, two lowest infrared modes A_{2u} and E_u shift by +7% and +3%, respectively.[2] The energies of other modes depend on u very weakly.

To analyze the effect of the SOC, we have compared the results obtained with and without the SOC calculated for $u = 0.06$ Å. As we see in Fig. 14, the strongest effect is found

[2]In the case of smaller displacements $u = 0.03$ Å numerical values of forces are too small, which may be the origin of some numerical error; therefore, we present phonon energies and dispersions obtained for $u = 0.06$ Å.

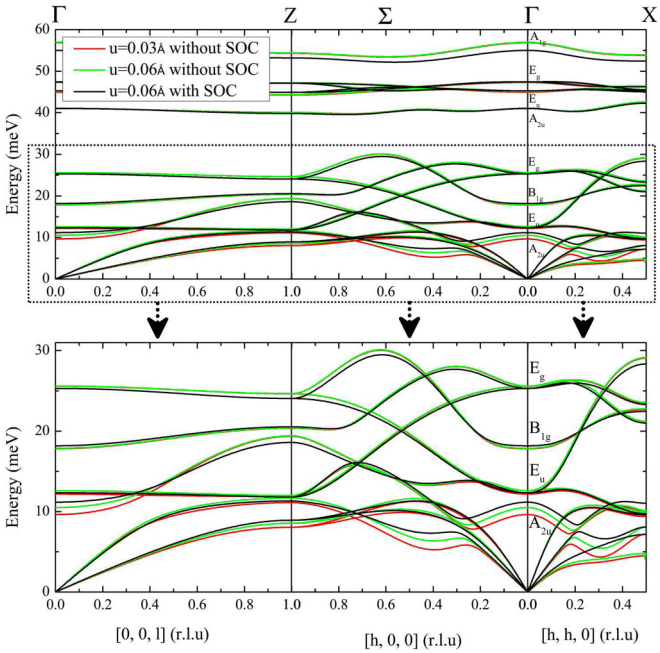

FIG. 14. (Color online) *Ab initio* calculation of the phonon dispersion curves along ΓZ, $\Gamma \Sigma Z$, and ΓX at 0 K. The parameter u sets for the displacements of the atoms. Increasing u from 0.03 Å (red line) to 0.06 Å (green line) is used to probe the effects of anharmonicity. Black line shows the calculation with spin-orbit coupling (SOC). The results of this last calculation ($u = 0.06$ Å and SOC) are the closest to the experimental results and are the ones reported in Fig. 13.

for the lowest infrared A_{2u} mode, which is shifted upward by 6.5% due to the SOC. The increase in energy in spite of larger lattice constants indicates a direct influence of the modified electronic structure on interatomic forces and phonon energies. Interestingly, the modes, which are strongly modified by the SOC, exhibit also the most pronounced dependence on u, and simultaneously they show the largest disagreement with the INS data (see Fig. 13 and Table I). The results obtained with the SOC and $u = 0.06$ Å, are slightly closer to the experimental points than the two other calculations. Generally, a good agreement between the theory and experiment is observed for most of dispersion curves, indicating the itinerant character of $5f$ electrons.

VII. GENERAL DISCUSSION AND CONCLUSION

Based on the observation of the same characteristic vector Q_0 in the HO and AF phase [25,26,58] (Brillouin zone folding from a bct to st) and the absence of lattice distortion across T_0, Harima *et al.* [59] have selected four subgroups of the group 139 as candidates for the lower space group of the HO state (Nos. 126, 128, 134, and 136); all have D_{4h} symmetry. Even without lattice distortion, across T_0, group theory predicts that new active phonon modes are allowed to emerge (B_{2g} phonon mode in the group Nos. 126, 134, and 136; only the group No. 128 doesn't have active B_{2g} phonon mode), some modes can be split (E_g or E_u modes) or new atoms are allowed to participate to the phonon movements (Uranium atoms in the E_g mode in group Nos. 126 and 134). None of these predictions have been observed here. Of course, the effects of the electronic transition on the lattice dynamics might be very limited. Quantitative calculations on the lattice dynamics based on precise electronic ordering at T_0 would be necessary to distinguish which effects would be sizable.

Recently, orthorhombic distortion upon entering the HO has been measured by x-ray scattering by Tonegawa *et al.* [29] in disagreement with results by Amitsuka *et al.* [60]. We do not observe any splitting or broadening of the phonons measured by Raman scattering or by optical conductivity measurements nor signs of the effect of the orthorhombic distortion on the in-plane acoustic phonons. But a quantitative comparison with the predictions based on this recent measurement and the width across T_0 as measured by optical spectroscopy would be necessary to definitively conclude.

In conclusion, we have performed Raman scattering, optical conductivity, inelastic neutron scattering measurements and *ab initio* calculations focused on the lattice dynamic properties of URu_2Si_2 in the 300 to 2 K temperature range. We have measured all the optical phonon modes at the center of the Brillouin zone (BZ) and we have followed almost all phonon branches below 30 meV in the main symmetry directions of the BZ, together with their temperature dependencies. No particular effect of the entrance into the hidden order state has been detected except a change in the Fano shape of the $E_u(2)$ phonon mode, a phonon which exhibits also a large increase of its spectral weight upon cooling from 300 K consistently with important electron-phonon coupling for this phonon. We attribute this behavior to the large loss of carriers upon entering the HO state. Other main effects have been obtained when entering into the Kondo regime. Indeed, we measure a small (0.5%) but sizable softening of the B_{1g} phonon mode below ~100 K. Most probably a complex electron-phonon coupling is in play, related to the Kondo physics. This and the previously reported softening of the elastic constant of the same symmetry observed by ultrasound velocity measurements strongly suggest a B_{1g} symmetry-breaking instability in the Kondo regime. The Kondo crossover also impacts the infrared-active $E_u(1)$ and $A_{2u}(2)$ modes. Both of them present a Fano shape but whereas the $A_{2u}(2)$ mode loses its Fano shape below 150 K, the $E_u(1)$ mode acquires it below 100 K, in the Kondo crossover regime. We attribute this behavior to strongly momentum-dependent Kondo physics. By drawing the full dispersion of the phonon modes and magnetic excitations, we conclude that there is no strong magnetoelastic coupling in URu_2Si_2. No remarkable temperature dependence has been obtained by INS, including through the hidden order transition. Thanks to polarized inelastic neutron scattering, we were able to distinguish between phonon and magnon modes near the X and Γ points of the BZ, shedding light on previous reports [33,61]. The *ab initio* calculations of phonon energies and polarization vectors allowed us for the detailed analysis of phonon modes in the zone center and along the high-symmetry directions. A good agreement between the theory and experiment is observed for most of dispersion curves. The discrepancy found for the lowest TA and TO modes propagating in the (a,b) plane may be caused by additional effects such as strong electron correlations, magnetic interactions, or relativistic effects not fully included in the present calculations.

ACKNOWLEDGMENTS

This work was supported by the Labex SEAM (Grant No. ANR-11-IDEX-0005-02) and by the French Agence Nationale de la Recherche (ANR PRINCESS). C.C.H. is supported by the US Department of Energy (DOE), Office of Basic Energy Sciences, Division of Materials Sciences and Engineering under Contract No. DE-AC02-98CH10886. The IT4Innovations National Supercomputing Center, VSB-Technical University, Ostrava, Czech Republic, is acknowledged for providing the computer facilities under Grant Reg. No. CZ.1.05/1.1.00/02.0070. We thank I. Paul, G. Knebel, C. Lacroix, and P. Oppeneer for very fruitful discussions.

[1] T. T. M. Palstra, A. A. Menovsky, J. van den Berg, A. J. Dirkmaat, P. H. Kes, G. J. Nieuwenhuys, and J. A. Mydosh, Phys. Rev. Lett. **55**, 2727 (1985).
[2] J. A. Mydosh and P. M. Oppeneer, Rev. Mod. Phys. **83**, 1301 (2011).
[3] J. Mydosh and P. Oppeneer, Philos. Mag. **94**, 3642 (2014).
[4] W. Schlabitz, J. Baumann, B. Pollit, U. Rauchschwalbe, H. M. Mayer, U. Ahlheim, and C. D. Bredl, Z. Phys. B Cond. Matter **62**, 171 (1986).
[5] A. de Visser, F. E. Kayzel, A. A. Menovsky, J. J. M. Franse, J. van den Berg, and G. J. Nieuwenhuys, Phys. Rev. B **34**, 8168 (1986).
[6] C. Broholm, H. Lin, P. T. Matthews, T. E. Mason, W. J. L. Buyers, M. F. Collins, A. A. Menovsky, J. A. Mydosh, and J. K. Kjems, Phys. Rev. B **43**, 12809 (1991).
[7] H. Kusunose and H. Harima, J. Phys. Soc. Jpn. **80**, 084702 (2011).
[8] K. Haule and G. Kotliar, Nature Phys. **5**, 796 (2009).
[9] H. Ikeda, M.-T. Suzuki, R. Arita, T. Takimoto, T. Shibauchi, and Y. Matsuda, Nature Phys. **8**, 528 (2012).
[10] J. G. Rau and H.-Y. Kee, Phys. Rev. B **85**, 245112 (2012).
[11] S. Fujimoto, Phys. Rev. Lett. **106**, 196407 (2011).
[12] P. S. Riseborough, B. Coqblin, and S. G. Magalhães, Phys. Rev. B **85**, 165116 (2012).
[13] T. Das, Phys. Rev. B **89**, 045135 (2014).
[14] C. Pépin, M. R. Norman, S. Burdin, and A. Ferraz, Phys. Rev. Lett. **106**, 106601 (2011).
[15] P. Chandra, P. Coleman, and R. Flint, Nature **493**, 621 (2013).
[16] S. Elgazzar, J. Rusz, M. Amft, P. M. Oppeneer, and J. A. Mydosh, Nat. Mater. **8**, 337 (2009).
[17] F. Bourdarot, E. Hassinger, S. Raymond, D. Aoki, V. Taufour, L.-P. Regnault, and J. Flouquet, J. Phys. Soc. Jpn. **79**, 064719 (2010).
[18] C. R. Wiebe, J. A. Janik, G. J. MacDougall, G. M. Luke, J. D. Garrett, H. D. Zhou, Y.-J. Jo, L. Balicas, Y. Qiu, J. R. D. Copley, Z. Yamani, and W. J. L. Buyers, Nature Phys. **3**, 96 (2007).
[19] A. Villaume, F. Bourdarot, E. Hassinger, S. Raymond, V. Taufour, D. Aoki, and J. Flouquet, Phys. Rev. B **78**, 012504 (2008).
[20] D. A. Bonn, J. D. Garrett, and T. Timusk, Phys. Rev. Lett. **61**, 1305 (1988).
[21] J. Schoenes, C. Schonenberger, J. J. M. Franse, and A. A. Menovsky, Phys. Rev. B **35**, 5375 (1987).
[22] T. T. M. Palstra, A. A. Menovsky, G. J. Nieuwenhuys, and J. A. Mydosh, J. Magn. Magn. Mater. **54–57**, 435 (1986).
[23] P. Aynajian, E. H. da Silva Neto, C. V. Parker, Y. Huang, A. Pasupathy, J. Mydosh, and A. Yazdani, Proc. Natl. Acad. Sci. USA **107**, 10383 (2010).
[24] G. W. Scheerer, W. Knafo, D. Aoki, G. Ballon, A. Mari, D. Vignolles, and J. Flouquet, Phys. Rev. B **85**, 094402 (2012).
[25] E. Hassinger, G. Knebel, T. D. Matsuda, D. Aoki, V. Taufour, and J. Flouquet, Phys. Rev. Lett. **105**, 216409 (2010).
[26] J. Buhot, M.-A. Méasson, Y. Gallais, M. Cazayous, A. Sacuto, G. Lapertot, and D. Aoki, Phys. Rev. Lett. **113**, 266405 (2014).
[27] R. Okazaki, T. Shibauchi, H. J. Shi, Y. Haga, T. D. Matsuda, E. Yamamoto, Y. Onuki, H. Ikeda, and Y. Matsuda, Science **331**, 439 (2011).
[28] S. Tonegawa, K. Hashimoto, K. Ikada, Y.-H. Lin, H. Shishido, Y. Haga, T. D. Matsuda, E. Yamamoto, Y. Onuki, H. Ikeda, Y. Matsuda, and T. Shibauchi, Phys. Rev. Lett. **109**, 036401 (2012).
[29] S. Tonegawa, S. Kasahara, T. Fukuda, K. Sugimoto, N. Yasuda, Y. Tsuruhara, D. Watanabe, Y. Mizukami, Y. Haga, T. D. Matsuda, E. Yamamoto, Y. Onuki, H. Ikeda, Y. Matsuda, and T. Shibauchi, Nature Commun. **5**, 5188 (2014).
[30] S. L. Cooper, M. V. Klein, Z. Fisk, and J. L. Smith, Phys. Rev. B **34**, 6235 (1986).
[31] T. Yanagisawa, S. Mombetsu, H. Hidaka, H. Amitsuka, M. Akatsu, S. Yasin, S. Zherlitsyn, J. Wosnitza, K. Huang, and M. Brian Maple, J. Phys. Soc. Jpn. **82**, 013601 (2013).
[32] K. Kuwahara, H. Amitsuka, T. Sakakibara, O. Suzuki, S. Nakamura, T. Goto, M. Mihalik, A. Menovsky, A. De Visser, and J. Franse, J. Phys. Soc. Jpn. **66**, 3251 (1997).
[33] N. P. Butch, M. E. Manley, J. R. Jeffries, M. Janoschek, K. Huang, M. B. Maple, and J. W. Lynn, arXiv:1212.6238.
[34] W. Hayes and R. Loudon, *Scattering of Light by Crystals*, Dover Books on Physics (Dover Publications, London, 2004).
[35] D. Aoki, F. Bourdarot, E. Hassinger, G. Knebel, A. Miyake, S. Raymond, V. Taufour, and J. Flouquet, J. Phys.: Condens. Matter **22**, 164205 (2010).
[36] J. Buhot, M.-A. Méasson, Y. Gallais, M. Cazayous, A. Sacuto, G. Lapertot, and D. Aoki, J. Korean Phys. Soc. **62**, 1427 (2013).
[37] P. G. Klemens, Phys. Rev. **148**, 845 (1966).
[38] J. Menéndez and M. Cardona, Phys. Rev. B **29**, 2051 (1984).
[39] S. L. Cooper, M. V. Klein, M. B. Maple, and M. S. Torikachvili, Phys. Rev. B **36**, 5743 (1987).
[40] D. Lampakis, D. Palles, E. Liarokapis, and J. Mydosh, Physica B (Amsterdam) **378-380**, 578 (2006).
[41] U. Nagel, T. Uleksin, T. Room, R. P. S. M. Lobo, P. Lejay, C. C. Homes, J. S. Hall, A. W. Kinross, S. K. Purdy, T. Munsie, T. J. Williams, G. M. Luke, and T. Timusk, Proc. Natl. Acad. Sci. USA **109**, 19161 (2012).
[42] W. T. Guo, Z. G. Chen, T. J. Williams, J. D. Garrett, G. M. Luke, and N. L. Wang, Phys. Rev. B **85**, 195105 (2012).
[43] J. Levallois, F. Lévy-Bertrand, M. K. Tran, D. Stricker, J. A. Mydosh, Y.-K. Huang, and D. van der Marel, Phys. Rev. B **84**, 184420 (2011).

[44] C. C. Homes, M. Reedyk, D. A. Cradles, and T. Timusk, Appl. Opt. **32**, 2976 (1993).
[45] L. Degiorgi, S. Thieme, H. R. Ott, M. Dressel, G. Grüner, Y. Dalichaouch, M. B. Maple, Z. Fisk, C. Geibel, and F. Steglich, Z. Phys. B Cond. Matter **102**, 367 (1997).
[46] U. Fano, Phys. Rev. **124**, 1866 (1961).
[47] L. C. Davis and L. A. Feldkamp, Phys. Rev. B **15**, 2961 (1977).
[48] H. Martinho, P. G. Pagliuso, V. Fritsch, N. O. Moreno, J. L. Sarrao, and C. Rettori, Phys. Rev. B **75**, 045108 (2007).
[49] J. Panarin, S. Raymond, G. Lapertot, J. Flouquet, and J.-M. Mignot, Phys. Rev. B **84**, 052505 (2011).
[50] N. P. Butch, M. E. Manley, J. R. Jeffries, M. Janoschek, K. Huang, M. B. Maple, A. H. Said, B. M. Leu, and J. W. Lynn, Phys. Rev. B **91**, 035128 (2015).
[51] G. Kresse and J. Furthmüller, Phys. Rev. B **54**, 11169 (1996).
[52] P. E. Blochl, Phys. Rev. B **50**, 17953 (1994).
[53] J. P. Perdew, K. Burke, and M. Ernzerhof, Phys. Rev. Lett. **77**, 3865 (1996).
[54] P. M. Oppeneer, J. Rusz, S. Elgazzar, M.-T. Suzuki, T. Durakiewicz, and J. A. Mydosh, Phys. Rev. B **82**, 205103 (2010).
[55] K. Parlinski, Z.-Q. Li, and Y. Kawazoe, Phys. Rev. Lett. **78**, 4063 (1997).
[56] K. Parlinski, Collection SFN **12**, 161 (2011).
[57] M. Hoesch, P. Piekarz, A. Bosak, M. Le Tacon, M. Krisch, A. Kozłowski, A. M. Oleś, and K. Parlinski, Phys. Rev. Lett. **110**, 207204 (2013).
[58] R. Yoshida, K. Tsubota, T. Ishiga, M. Sunagawa, J. Sonoyama, D. Aoki, J. Flouquet, T. Wakita, Y. Muraoka, and T. Yokoya, Sci. Rep. **3**, 2750 (2013).
[59] H. Harima, K. Miyake, and J. Flouquet, J. Phys. Soc. Jpn. **79**, 033705 (2010).
[60] H. Amitsuka, Workshop on Hidden Order, Superconductivity, and Magnetism in URu_2Si_2, Leiden, 2013 (unpublished).
[61] C. Broholm, J. K. Kjems, W. J. L. Buyers, P. Matthews, T. T. M. Palstra, A. A. Menovsky, and J. A. Mydosh, Phys. Rev. Lett. **58**, 1467 (1987).